Target Recognition by Catechols and β-Ketoenols: Potential Contribution of Hydrogen Bonding and Mn/Mg Chelation to HIV-1 Integrase Inhibition

Luba Tchertanov* and Jean-François Mouscadet

Laboratoire de Biotechnologie et Pharmacologie Génétique Appliquée, CNRS UMR 8113, Ecole Normale Supérieure de Cachan, 61 av. Président Wilson, 94235 Cachan, France

Received November 29, 2006

Catechol and β-ketoenol are important pharmacophores of HIV-1 integrase (IN) inhibitors. We investigated their recognition of the divalent metals, Mg and Mn, and of hydrogen bond donors (HBD) and acceptors (HBA). We used data retrieved from the Cambridge Structural Database (CSD), applying a 3-D structure-based, *in silico*-driven approach. We found that both biophores were stabilized by intramolecular H-bonding (IHB), which was weak in catechols and very strong in β-ketoenols. Catechols tended to recognize environmental HBD and HBA, demonstrating their ability to make use of both hydroxyl groups to form multiple, strong intermolecular H-bonds. In contrast, β-ketoenols stabilized by strong IHB inefficiently formed intermolecular H-bonds. β-Ketoenolate chelated both Mg and Mn ions much more efficiently than dioxolene, which was highly selective for Mn cations. The significant differences in the ability of these two pharmacophores to bind HBD and HBA and in their ability to chelate Mg and Mn have important consequences for competitive inhibitor binding and selectivity for metals and integrase DNA-binding sites.

Introduction

Antiviral drug development requires detailed information about the biological activity of the pharmacological compounds against selected targets. At the molecular level, the biological activity of a molecule is determined by its binding (recognition and affinity) to a target, usually a protein or macromolecular assembly, such as a protein/protein or protein/nucleic acid (DNA or RNA) complex. The forces driving the binding process are weak, short-range, noncovalent interactions (hydrogen bonding, electrostatic, and hydrophobic interactions) requiring the molecular partners to fit both chemically and geometrically. In metal-dependent enzymes, such as polynucleotidyl transferases, which require Mn or Mg for their activity *in vitro*, the recognition process may also involve interactions of the inhibitor with divalent metals. The HIV-1 integrase (IN[a]) belongs to this family of enzymes. It catalyzes the integration of a DNA copy of the viral genome into the chromosomal DNA, an essential step in viral replication, and therefore constitutes an attractive target for antiviral chemotherapy. HIV-1 IN is a 32-kDa protein (288 amino acids) with three different functional domains: the N-terminal domain (residues 1−49), which contains a nonconventional HHCC zinc-finger motif, the central core (residues 50−212), and the C-terminal domain (residues 213−288). The binding of Zn^{2+} to the HHCC motif has been shown to promote IN polymerization *in vitro*[1,2]. The central core, which is also known as the catalytic core domain, contains the canonical DDE motif conserved among retroviral integrases, a number of bacteriophage transposases, and the Holliday junction RuvC resolvases.[3,4] These amino acid residues (Asp64, Asp116, and Glu152) form a divalent metal-binding site, which recognizes cations such as Mg^{2+} and Mn^{2+}. Crystal structures containing only one divalent cation have been observed, but, by analogy with other retroviral integrases and with the proposed mechanism of action of polynucleotidyl transferases, we would expect two metal cations to be required for the formation of an active complex between HIV-1 IN and its DNA target.[5] The integrase C-terminal domain, which displays nonspecific DNA-binding activity, is involved in stabilizing the integrase−DNA complex.[6−9]

Over the years, a large number of compounds, including peptides, oligonucleotides, and small organic molecules, have been reported to inhibit IN (reviewed in refs 10−13). Most of the compounds initially identified as IN inhibitors were polyhydroxylated aromatic compounds.[14−16] Studies on natural (chicoric acid) and synthetic (caffeic acid) polyphenols identified catechol as a functional pharmacophore.[17] Catechol-containing compounds were the first class of IN inhibitors to be identified, blocking both IN activity and IN binding to viral DNA. β-Ketoenols were recently identified as an another promising group of pharmacophores with potent anti-integrase activity (or INBI).[18−20] This pharmacophore is optimized further in hydroxyquinolines, on which the most advanced compounds of this type yet developed, naphthyridine carboxamides, are based.[18,21] Pharmacophores of this type belong to a second class of IN inhibitors blocking the second step in integration. They are therefore known as IN strand transfer inhibitors (INSTI).

Catechols, ketoenols, and hydroxyquinolines are thought to be involved in metal chelation. This suggests that the formation of a metal−ligand coordination complex with one or two divalent ions is a key factor in the inhibition of IN.[22−25] The only available X-ray structure of the catalytic core domain of IN with a β-ketoenol inhibitor (5CITEP) shows the inhibitor located within the active site, not bound to Mg^{+2} but interacting with E152 *via* the two oxygen atoms of β-ketoenol, through two H-bonds.[19] Other results concerning inhibitor binding were obtained by docking probes on crystallographic models[26−35] or on the theoretical model of full-length HIV-1 integrase complexed with viral DNA.[36] Different orientations of inhibitors in the binding site of HIV-1 IN and different modes of interaction have been proposed, but the Mg^{2+} ion has generally been reported to be chelated by the diketo group.

* To whom correspondence should be addressed. Phone: +33 1 47407662; Fax: +33 1 4740 7684; E-mail: luba.tchertanov@lbpa.ens-cachan.fr.

[a] Abbreviations: IN HIV-1, integrase human immunodeficiency virus type 1; HBD, hydrogen bond donor; HBA, hydrogen bond acceptor; IHD, intramolecular hydrogen bond; RAHB, resonance-assisted hydrogen bonding; CSD, Cambridge Structural Database; M, metal; L1, β-ketoenolate; L2, dioxolene.

10.1021/jm061375j CCC: $37.00 © 2007 American Chemical Society
Published on Web 02/16/2007

Chart 1. Catechol (I) and β-Ketoenol (II) Structural Motifs

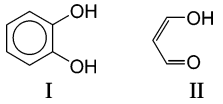

Chart 2. Structural Conformers of Catechol

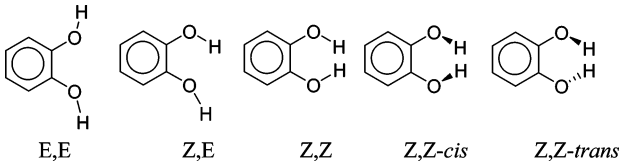

Secondary pharmacophores are not required for anti-integrase activity but do seem to be required for target selectivity, as they are involved in the establishment of ancillary interactions with the amino acid residues of the protein. Both catechol and β-ketoenol pharmacophores are present in chimeric compounds blocking both steps, although this inhibition is not as efficient as that mediated by strand transfer inhibitors.[31,37−39] The behavior of styrylquinolines is intermediate between that of INSTI and catechol-based compounds. These inhibitors, which have more than one active function, may have to compete for receptor sites because their binding is driven by strongly specific and competitive interactions.[40] Drug optimization therefore requires a comparative description of the binding and affinity of each molecular fragment involved in target recognition, shedding light on preferences for fragment-target interaction in a specified environment.[41] We focus here on catechol (I) and β-ketoenol (II) (Chart 1). These key functional pharmacophores are the main building blocks for a large number of antiviral inhibitors and may both be present in the same molecule.

Both molecular entities are bidentate, oxygen-based, polyfunctional ligands able to bind various agents, metal ions, hydrogen-bond donors (HBD), and hydrogen-bond acceptors (HBA). We investigated the molecular recognition properties of inhibitors based on catechol and β-ketoenol and tried to distinguish between the binding possibilities of these molecules, using the Cambridge Structural Database (CSD),[42,43] an abundant source of accurate data for small molecular structures. We applied univariate and bivariate analysis[44] to experimental 3-D structural data, to obtain a quantitative description of the structural properties and affinity of the chosen pharmacophores. We first analyzed the conformational properties of these two molecular entities. We assessed the ability of catechols and β-ketoenols to recognize their environment, by determining the number of H-bond partners, strength of interaction, and spatial arrangement of HBA and HBD groups on each molecular entity. Finally, a comparative analysis of the binding of these pharmacophores to magnesium and manganese provided insight into the particular features of metal recognition by catechol and β-ketoenol and made it possible to compare the functional roles of these ligands in inhibition involving a divalent metal cation.

Results and Discussion

Structure of Catechols. Catechol (1,2-dihydroxybenzene) can adopt more than one conformation, according to the orientation of the two hydroxyl groups (Chart 2). Theoretical analysis (*ab initio* and semi-empirical quantum mechanics calculations) suggests that there are two stable catechol conformers: *E,E*- and *Z,E*.[45] In the *E,E*-conformer, the hydrogen atoms of the hydroxyl groups point away from each other, whereas in the *Z,E*-conformer, the synclinal position of one hydroxyl group favors the formation of an intramolecular

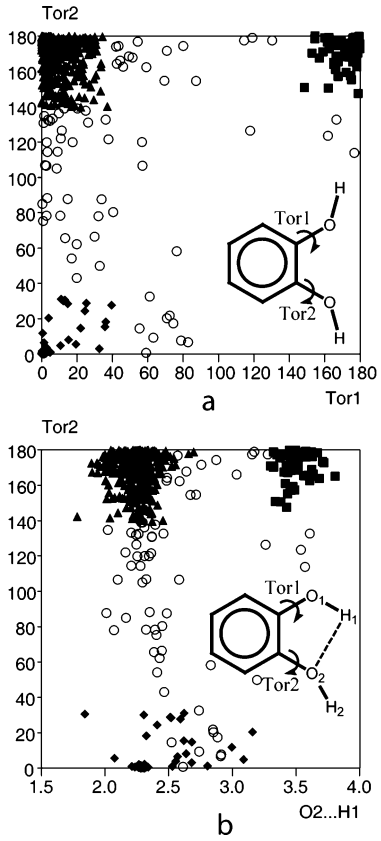

Figure 1. Conformations and intramolecular H-bonding in 601 catechol fragments from 286 crystal structures. (a) Scatter plots of absolute value of torsion angles, Tor1 vs Tor2, describing the positions of OH groups relative to the adjacent aromatic C−C bond, as defined in the inset; (b) Absolute value of torsion angle Tor2 vs intramolecular distance H1···O2. The *E,E*- (squares ■), *Z,E*- (triangles ▲) and *Z,Z*- (diamonds ◆) conformations are indicated by closed symbols. Intermediate conformations are shown as hollow symbols (○). The *Z,E*- and *E,Z*-conformations could not be distinguished either chemically or structurally and are represented as a unique *Z,E*-cluster.

O−H...O hydrogen bond. *Ab initio* calculations indicate that the planar *Z,E*-conformation about 5 kcal mol^{-1} is more stable.[46,47]

We analyzed the conformational and recognition properties of catechols and their derivatives in crystals. The torsion angles Tor1 and Tor2, describing the positions of OH groups relative to the adjacent aromatic C−C bond, were used to distinguish between catechol conformations. A scatter plot of absolute values of torsion angles (Tor1 vs Tor2) revealed three dense clusters and a limited number of randomly distributed observations (Figure 1a). Torsion angles within the ranges 0° to 40° and 140° to 180° were considered to meet the criteria for *Z*- and *E*- conformations, respectively. On the basis of this definition, the three distinct clusters observed for the entire set of experimental data were attributed to the *E,E*- (Tor1 and Tor2 ∼ 180°), *Z,E*- (Tor1 ∼ 0° and Tor2 ∼ 180°), and *Z,Z* (Tor1 ∼ 0° and Tor2 ∼ 0°) catechol conformations. The clusters were distinguished by the use of distinct symbols, and this notation was retained for subsequent statistical analysis. The randomly distributed points (open circles) corresponding to intermediate conformations were included in the subsequent analysis but were not considered in the interpretation. The populations of the different clusters were not identical, with most of the catechols deposited in the CSD adopting *Z,E*- conformations (65%) and only 18% adopting *E,E*- and 7% adopting *Z,Z*-conformations. The intramolecular H···O distance was strongly correlated with

catechol conformation (Figure 1b). In *Z*,*E* catechols, the H···O distance ranges from 1.78 to 2.55 Å and corresponds to stabilizing intramolecular H-bonding (IHB) between the O−H group in the *Z* conformation as a donor and the oxygen atom of the O−H group in the *E* conformation as an acceptor. Assuming that the length of a hydrogen bond is correlated with its strength, intramolecular O···H distances (mean value (mv) with standard error (SE) of 2.25(1)) in *Z*,*E*-catechols and pseudo angle at the H-atom (mv of 110.4(6)°) suggest that this interaction corresponds to a moderate or more probably weak intramolecular H-bond. The well localized positions of the hydrogen atoms relative to the oxygen atoms indicates that these interactions are mostly electrostatic, with a frozen proton-transfer event.[48] In catechols with a *Z*,*Z*-conformation, which is not stable in the gas phase and is rare in crystals, H···O distances (mv of 2.36(2) Å) probably correspond to repulsive interactions between the vicinal hydroxyl groups, both of which are in synclinal conformation. This hypothesis is confirmed by the greater distance between the oxygen atoms in *Z*,*Z* catechols than in other conformers (mv O···O of 2.78(1) Å in *Z*,*Z*- vs 2.675(2) Å in *Z*,*E*- and *E*,*E*-forms). In *E*,*E*-catechols, which have hydroxyl groups oriented in opposite directions, H···O distances are very large (from 3.30 to 3.70 Å).

Thus, structural analyses of catechols and their derivatives indicate that all conformations of catechol occur in crystals but with different frequencies, *Z*,*E* being much more frequent than *E*,*E*, which is in turn more frequent than *Z*,*Z*. The *Z*,*E*-conformation is stabilized by moderate or weak intramolecular H-bonding between two hydroxyl groups, with one, in *Z*-conformation, acting as a donor, and the other, in *E*-conformation, acting as an acceptor.

Intermolecular Hydrogen Bonding of Catechols in Crystals. We assumed that different catechol conformations have different hydrogen bonding and recognition patterns. We expected to observe major differences between catechols stabilized by intramolecular H-bonds and other catechols, because the most common reason for missing intermolecular H-bonds is the formation of intramolecular contacts. Competition between intra- and intermolecular hydrogen bonding is one of the factors affecting the ability of strong donors and acceptors to recognize neighboring HBD or HBA groups.[49,50] We describe the catechol recognition of HBD and HBA environments based on the involvement of oxygen- or nitrogen-containing molecular fragments: H−O/N and O/N, respectively. Two types of intermolecular H-bonding are observed between catechol and such targets: with catechol serving as the donor in one and as the acceptor in the other. In each case, the donor function is fulfilled by the two hydroxyl groups and the acceptor function is filled by the two oxygen atoms.

Catechol acts as the proton donor in intermolecular H-bonding, O−H···O/N, in 84% of cases. The exceptions to this rule are cases in which the catechol is involved in intramolecular H-bonding with a non-catechol acceptor group or intermolecular H-bonding with halogen or sulfur atoms, which was not considered here. Intermolecular contacts indicative of catechol acting as an acceptor, O···H−(O/N), were observed in 65% of catechol structures. The remaining structures showed an absence or lack of potential HBDs. All H-bond contacts, O−H···O/N and O···H−(O/N), satisfying H-bond criteria[51] were characterized by commonly used measures: distances between interacting atoms (donor···acceptor and H···acceptor) and the pseudo valent angle at the H-atom involved in the interaction. H-bond contacts were not analyzed as a function of the nature of the partner atom, as only 4% of HBAs and 6% of HBDs were nitrogen-based molecular fragments, with all others being oxygen-based groups. We therefore processed all the data together.

The catechol participating as a hydrogen bond donor in O−H···O/N interactions forms H-bonds of various strengths, from strong and linear to moderate and weak (Figure 2a,b). The H···O/N distance ranges from 1.58 to 2.72 Å and is positively correlated (correlation coefficient *r* of 0.73) with the O···O/N distance, which ranges from 2.55 to 3.05 Å. A scatter plot of H···O/N distance vs the angle at the H-atom showed a comet-like distribution (*r* of −0.86) with a dense "nucleus" centered in the range of linear angles at the H-atom (160−180°) and short O···H distances (1.6−1.8 Å) corresponding to strong H-bonding. The middle part of the "comet" corresponded to moderate H-bonding, and the tail to weak and dispersed H-bonding. The data indicate that all catechol conformers act as donors in intermolecular H-bonding, although several important features must be taken into account. The points in the dense "nucleus" of the comet-like distribution correspond mostly to cases of H-bonding involving catechols in the *E*,*E*- and *Z*,*E* conformations. For *E*,*E*-catechols, H-bonding is strong and linear in most cases. For catechols stabilized by intramolecular H-bonding, the OH group in the *E* position seems to be a better hydrogen-bond competitor than that in the *Z* position, forming stronger, linear H-bonds. As expected, the role of the group in the *Z* position as a proton donor in intramolecular H-bonding appears to be the main factor underlying the relative weakness of intermolecular O−H···O/N hydrogen bonds.

Intermolecular H-bonds in which catechol acts as an acceptor differ from those in which it acts as a donor (Figure 2a−d). In particular, the O···O/N and O···H bond distances are longer (mv of 2.845(5) and 2.09(1) Å *versus* mv of 2.774(5) and 1.926(9) Å for catechols acting as donors; Table 1). Large differences were also observed in the linearity of these contacts; the mv of angles at the H-atom of 138.0(8)° corresponds to a marked deviation from the linearity of O···H−(O/N) hydrogen bonds, with values of 150.2(8) Å recorded for O−H···O/N bonds. H···O/N distances were found to be perfectly correlated with angles at the H-atom (*r* of −0.89), but the "nucleus" on the scatter plot, characterizing the most populated domain, was displaced toward a range of 1.8−2.2 Å for O···H−(O/N) distances and 140−170° for the pseudo valent angle at the H-atom. Finally, the non-uniform distribution of points corresponding to interactions of OH groups in the *E*- and *Z*-positions clearly indicated a tendency of the hydroxyl groups in the *Z*-position in *Z*,*E*-catechols to bind more tightly to the HBD than those in *E*-conformations.

The structural data clearly show that catechols involved in intermolecular H-bonding bind HBDs less tightly than HBAs. However, the number of O···H−(O/N) and O−H···O/N contacts per catechol is almost identical in both cases. Interestingly, 8% of all O···H−(O/N) bonds correspond to bifurcated (three-centered) hydrogen bonding.[48,51] This percentage is about twice that of bifurcated O−H···O/N hydrogen bonding for catechols acting as hydrogen bond donors.

Catechols involved in intermolecular H-bonding use both hydroxyl groups. The hydroxyl group in the *Z* position appears to be a more effective hydrogen-bond competitor in O···H−(O/N) interactions than that in the *E* position, whereas the *E*-hydroxyl group is the better competitor in O−H···O/N interactions, forming stronger, more linear H-bonds than the OH-group in the *Z* position. The intramolecular hydrogen bond O−H···O stabilizing the *Z*,*E*-conformation is thus too weak to prevent the recognition of hydrogen bond groups, on HBD or HBA, by catechol. However, this IHB has a significant effect

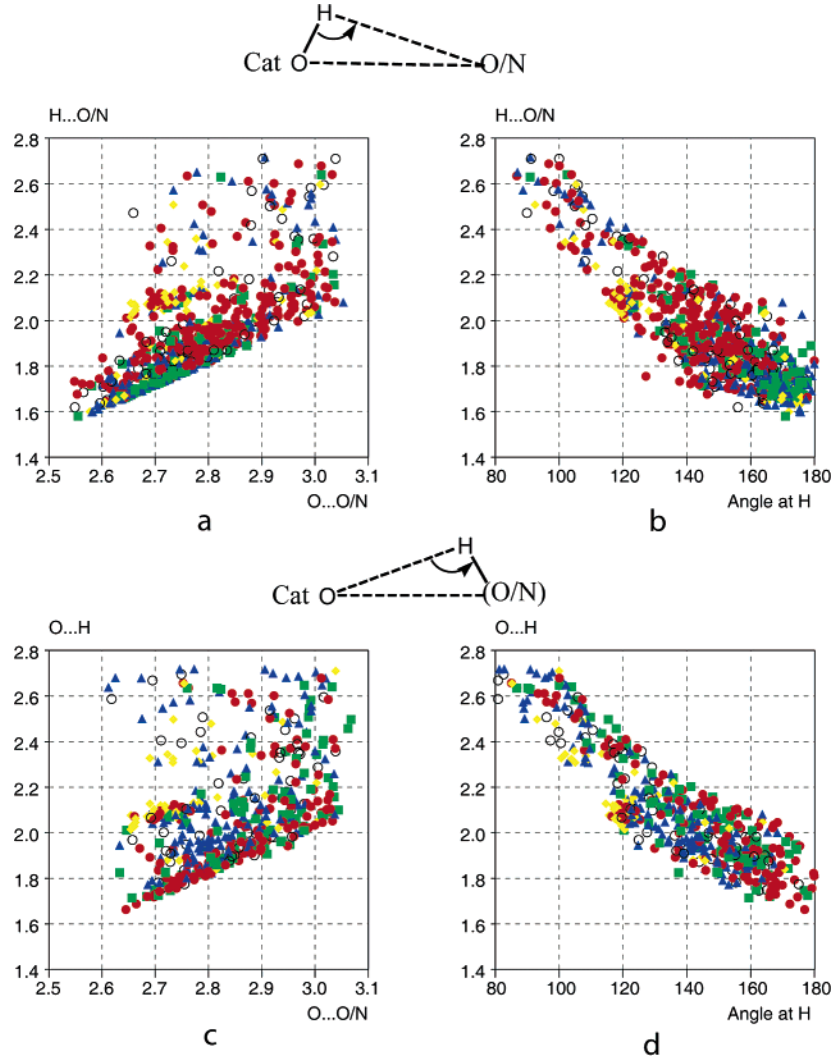

Figure 2. Intermolecular H-bonding of catechol. Top: Catechol acts as a donor in 239 of 286 structures forming 596 crystallographically independent and 646 symmetry-related O−H···O/N contacts. **(**a**)** Scatter plots of O···O/N vs H···O/N and **(**b**)** pseudo valent angle at the H-atom vs H···O/N. Bottom: Catechol acts as an acceptor in 187 of 286 structures forming 566 independent and 608 symmetry-related O···H−(O/N) contacts. (c) Scatter plots of O···O/N vs O···H and **(**d**)** pseudo valent angle at the H-atom vs O···H. Conformation *E*,*E*- (green squares); *Z*,*Z*- (yellow diamonds); *Z*,*E*- : (red circles) and (blue triangles) for the *Z*- and *E*-OH groups, respectively.

on the selectivity of *E*- and *Z*-hydroxyl groups and on the strength of intermolecular interactions. In both interactions, O−H···O/N and O···H−(O/N), the main targets are the oxygen-based agents, O-based donor or acceptor groups.

Catechol−Water Interactions. The avidity of catechol for oxygen-based partners led us to investigate the binding of catechol to water, which might act as a competitor in biological systems.[52−54] A recent computational study of catechol−water clusters (BLYP/6 31+G** level of theory) predicted various conformers.[55] The most stable structure was found to be *Z*,*E*-catechol, in which one (*E*-position) of the two hydroxyl groups donates a proton to the water molecule. In the next most stable catechol−water cluster structure, the water molecule interacts with the two OH groups of *Z*,*Z*-catechol. One of the OH groups acts as a proton donor, with the other acting as a proton acceptor, giving significantly weaker hydrogen bonding. The third most stable isomer cluster contains *Z*,*E*−catechol, with the *Z*-oriented OH group acting as the acceptor of a proton from the water molecule. We compared these predicted clusters with the catechol−water interaction in crystallohydrates representing more than 40% of all catechol crystal structures (122 of 286 structures). We found that the water molecule was generally located very close to the catechol and was positioned either between the two O−H groups of the catechol (30 structures), or closer to one of these groups (57 structures).

In the first type of clusters, the water molecules located between the two hydroxyl groups form a single H-bond with catechol, the establishment of a second contact generally being sterically impaired. Only in a few structures of this type does the catechol really chelate the water molecule: *E*,*E*-catechol interacts *via* symmetric bifurcated O···H−O bonds sharing one H-atom of the water, whereas *Z*,*Z*-catechol captures the water oxygen by forming O−H···O bonds, with both H-atoms of the water molecule then being directed outward from the catechol.

In the second type of clusters, the water molecules positioned at only one of the hydroxyl groups of catechol act as a HBA with OH groups in the *E* position and as a HBD with OH groups in the *Z* position. Catechol therefore seems to chelate water inefficiently, preferring other oxygen-based agents, such as hydroxyl (OH) and carbonyl (C═O) groups.

Multiple H-Bonding and Directionality. In the solid state, 90% of all catechols are involved in intermolecular H-bonding with oxygen- or nitrogen-based agents, either HBA or HBD, and about 80% are involved in intermolecular H-bonding, as simultaneous donors and acceptors, as illustrated in Figure 3. The structures ATUZOE, SEFRIE, and MXPHIQ01 (CSD entry

Table 1. Intra- and Intermolecular H-Bonds in Catechols and β-Ketoenols[a]

parameter	catechols	β-ketoenols
Intramolecular H-Bond O···H−O[b]		
O···O, Å	2.675(2)	2.554(2)
O···H, Å	2.25(1)	1.727(4)
∠O···H−O, deg	110.4(6)	147.0(2)
Intramolecular H-Bond O−H···Acceptor[c]		
O···O/N, Å	2.774(5)	2.900(6)
H···O/N, Å	1.926(9)	2.40(1)
∠O-H···O/N, deg	150.2(8)	115.9(9)
Intermolecular H-Bond O(H)···H-Donor[c]		
O···O/N, Å	2.845(5)	2.834(5)
O···H(O/N), Å	2.09(1)	2.10(3)
∠O···H−(O/N), deg	138.0(8)	146.6(1)
Intermolecular H-Bonds C═O···H-Donor[c]		
O···O/N, Å		2.874(7)
O···H(O/N), Å		2.24(1)
∠O···H−(O/N), deg		134.9(1)

[a] Mean values (mv) with standard errors (SE) for the distance between donor and acceptor atoms, O···O/N; the distance between the H-atom and acceptor atom, H···O/N and O···H(O/N); the pseudo valent angle at the H-atom, ∠O···H−(O/N) and ∠O−H···O/N. [b] *Z,E*-Catechols and *Z*-β-ketoenols were considered. [c] All catechols and *Z*-β-ketoenols were considered.

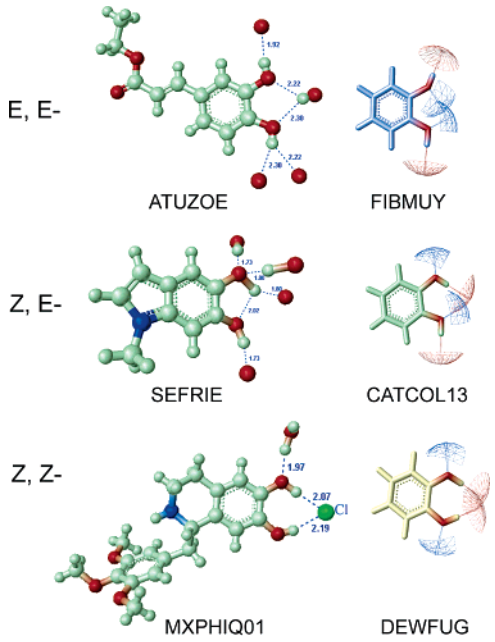

Figure 3. Multiple H-bonding of catechol. Left: H-bonds in *E,E*- (ATUZOE), *Z,E*- (SEFRIE), and *Z,Z*- (MXPHIQ01) catechol structures are shown as dotted lines, together with bond distances between the H-atom and acceptor. Right: Donor (blue) and acceptor (red) surfaces of nonsubstituted catechols were recovered from high-resolution crystal structures (FIBMUY (*E,E*), CATCOL13 (*Z,E*), and DEWFUG (*Z,Z*)) and viewed with Benchware 3D Explorer. The structures are referenced, together with their CSD refcode.

codes) correspond to the molecules based on catechol in *E,E*-, *Z,E*-, and *Z,Z*-conformations, respectively, and demonstrate the outstanding ability of catechol to recognize multiple HBD and HBA agents simultaneously. In ATUZOE, both OH groups act as donors in intermolecular H-bonding, with one of these groups forming a single, strong, linear H-bond and the other involved in almost symmetric H-bonding with two acceptor groups (bifurcated H-bonding). Moreover, both the oxygen atoms of catechol are bound to the same donor (OH group), providing a further example of bifurcated H-bonding. Thus, catechol intermolecular H-bonding in ATUZOE consists of five H-bonds, with four partners, three acceptors, and a single donor group. Two pairs of bifurcated H-bonds are formed simultaneously, with catechol acting as a donor in the first three-centered H-bond and as an acceptor in the second. All the binding partners of catechol in ATUZOE are oxygen-based functional groups. In SEFRIE the *Z,E*-conformation of catechol is characteristically stabilized by an intermolecular H-bond. The *Z*-oriented O−H group acting as a donor in IHB also acts as a donor and as an acceptor in intermolecular H-bonding, resulting in a complex environment with three H-bond partners. Thus, the *Z*-hydroxyl group acting as a donor in IHB retains its ability to recognize two categories of partners, HBD and HBA, resulting in the formation of strong intermolecular H-bonds. This OH group is involved in four H-bonds performing two important functions: stabilizing the *Z,E*-conformation of the catechol and recognizing the acceptor and donor groups in the immediate environment. The OH-group in the *E*-conformation, which acts as an acceptor in IHB, also forms strong, linear intermolecular H-bonds with HBA. The MXPHIQ01 structure corresponds to a rare *Z,Z*-conformation of catechol, with two hydroxyl groups oriented "zusammen". The catechol fragment is planar, and steric strain is relieved by increasing the O···O distance to 2.94 Å, the mean O···O distance being 2.675(2) Å in *Z,E*- and *E,E*-catechols. The H···H distance of 2.18 Å indicates that the system remains significantly strained. This conformation is probably stabilized by the strong intermolecular H-bonds formed with the chloride anion by both OH groups. This provides another example of bifurcated H-bonding, with catechol OH groups acting as donors and interacting, in this case, with the electronegative ion. We excluded electronegative species, such as halogens, from our statistical analysis, due to their unusual nature and considerable differences from oxygen- and nitrogen-based acceptor groups. The interactions of these species with catechol are nonetheless of particular interest, and detailed analyses would improve our understanding of catechol recognition and affinity.

An analysis of structural data for catechol H-bonding showed that the catechols in *E,E*-, *E,Z*-, and *Z,Z*-conformations tended to recognize environmental HBDs and HBAs and to form particularly strong intermolecular H-bonds. Catechol may act as both donor and acceptor, forming multiple H-bonds. We carried out statistical analyses to estimate the number of intermolecular hydrogen bonds (i.e., the "statistical" coordination number) formed by catechol. We found that the coordination number of the OH groups ranged between one and four. The total number of intermolecular H-bonds was between two and six *per* catechol. The number of hydrogen bonds depends on the presence of potential H-bond acceptors and H-bond donors; the number of hydrogen bonds is minimal in poor environments, whereas catechol can bind to a large number of partners, forming a branched hydrogen bond network, in exceptionally favorable environments.

The exceptional ability of catechol to participate in multiple intermolecular H-bonding makes it possible to investigate the spatial geometry of catechol OH-groups encircled by environmental HBD and/or HBA, with characterization on the basis of donor and acceptor directionality. In O−H···O/N interactions the main feature distinguishing hydrogen bonds from van der Waals interactions is the preference for linearity.[48] HBA should therefore be oriented with respect to the OH group of catechol OH such that this criterion is satisfied. The position of the HBA is therefore correlated with catechol conformation. HBAs forming strong, linear H-bonds with OH groups in the *E* position are inclined toward the oxygen of the catechol, forming an angle at the O-atom of 111.2(3)°, whereas HBAs forming weak

Chart 3. Structures of Representative HIV-1 IN Inhibitors: S-1360[61] (II-1), L-870,812[21] (II-2), and Thalassiolin A[62] (II-3), Based on β-Ketoenol Fragments in Which All the Carbon Atoms are Aliphatic (II-1), the Carbonyl Carbon Atom is Aliphatic, and the Others are Aromatic (II-2) or All the Carbon Atoms are Aromatic (II-3)

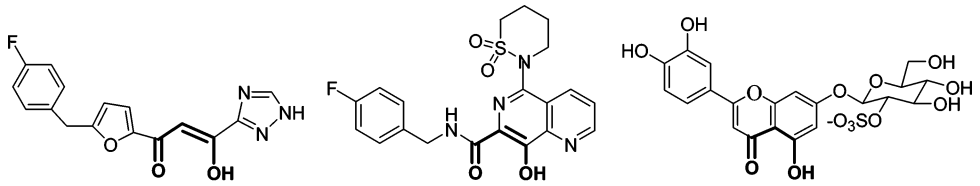

hydrogen bonds (typically for OH groups in the *Z* position) form a larger angle at the O-atom (120 to 140°). In O···H−O/N interactions (acceptor directionality), the direction is identical to that for a hypothetical proton-transfer reaction (the lone pair direction).[48] The diffuse electron density of oxygen atoms favors a linear geometry for hydrogen bonds. Indeed, HBDs forming strong, linear H-bonds display preferential positioning such that the angle at the O-atom is either 109 or 120°. The spatial arrangement of HBD and HDA agents around the hydroxyl group of catechol therefore suggests two possible coordinations: tetrahedral and trigonal. The simulated surfaces of HBA and HBD agents around catechols in the *E*, *E*-, *Z*, *E*-, and *Z*, *Z*-conformations are presented in the right-hand column of Figure 3.[56]

Extensive hydrogen bonding may have a significant effect on the intramolecular covalent metrics of molecules or molecular moieties involved in this bonding, as shown for oxymes (C═N−O−H),[57] azides (N═N═N), and thiocyanates (S−C═N).[58−60] The expected elongation of the C−O bond attaching hydroxyl groups involved in multiple H-bonds is difficult to confirm systematically, probably due to interplay between diverse steric and electronic factors affecting the structure and properties of catechol.

Structure of β-Ketoenols. The hydroxyl and carbonyl group-containing moieties in the cis-configuration are separated by only one carbon atom: O═C−C═C−OH. This structural fragment is very common in chemically and structurally diverse small molecules, constituting the main building block for most known IN inhibitors.

Three main families can be formally distinguished, according to the nature of the carbon atoms (aliphatic or aromatic): β-ketoenols (II-1), α-acylphenyl derivatives (II-2), and β-ketoenol-like fragments inserted into bicyclic ring system (II-3), as illustrated in Chart 3, which displays some representative drug candidates.

These molecules differ both chemically and structurally. We investigated the structure and recognition properties of the fragment common to all these structures, O═C−C═C−OH (referred to as β-ketoenol for simplicity), to gain insight into potential binding modes. We also tried to distinguish the general properties of the common fragment from properties specific to the different families of molecules.

Structural data analysis (2147 β-ketoenol fragments from 1562 crystal structures) showed that, in the vast majority (96%) of β-ketoenols, the OH group adopts the *Z*-conformation and is stabilized by intramolecular H-bonding, resulting in the formation of a planar six-membered pseudo-ring =C−O−H···O═C−C (Figure 4**a**). *Ab initio* studies at the B3LYP/3-G** level of theory have predicted that the IHB stabilizes the energetically favorable *Z*-form of aliphatic β-ketoenols.[63] The intramolecular hydrogen bonding of this form was studied extensively in crystal structures by V. Bertolasi et al.,[64] who demonstrated that aliphatic β-ketoenols often form abnormally strong IHB, due to unusual π-delocalization of the O═C−C═C−OH heteroconjugated system. This phenomenon was interpreted in terms of resonance-assisted hydrogen bonding (RAHB), with particular attention paid to the study of intramolecular proton-transfer effects (PTE).[65,66]

We first investigated the occurrence of these two effects in the three families of β-ketoenols stabilized by IHB. We found that O···O and O···H distances and the pseudo valent angle at the H-atom (mv of 2.554(2), 1.727(4) Å, and 147.0(2)°, respectively) were characteristic of strong intramolecular H-bonding and differed significantly from those in *Z*,*E*-catechols (mv 2.675(2), 2.25(1) Å, and 110.4(6)°) (Table 1). We found that most of the structures with IHB satisfying the RAHB criteria (O···O ≤ 2.70, O···H ≤ 2.0 Å)[67] (94% of all β-ketoenols stabilized by IHB) displayed considerable electron density delocalization for the O═C−C═C−OH fragment. We can

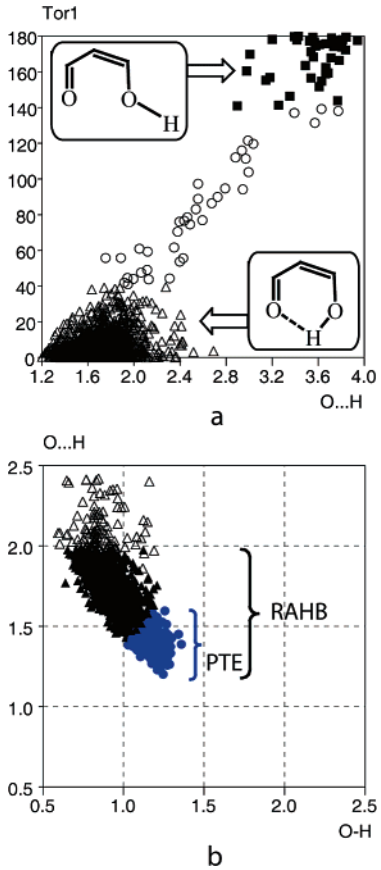

Figure 4. Conformation and intramolecular H-bonding of β-ketoenols observed in 2147 O═C−C═C−OH fragments from 1562 structures. Scatter plots of **(a)** O···H vs absolute value of torsion angle Tor1 and **(b)** O···H vs O−H, *r* of −0.77; *E*-conformation (36 observations, ■); *Z*- (2066 observations, △); intermediate **(○)**; H-bonded fragments satisfying RAHB criteria (O···O ≤ 2.70, O···H ≤ 2.0 Å) (1951 observations, ▲); H-bonded fragments satisfying RAHB and PTE criteria simultaneously (206 observations, blue circles).

Table 2. Intramolecular H-Bond Parameters and Covalent Bond Lengths in the O═C−C−C−OH Fragment of β-Ketoenols[a]

parameter	all[b]	RAHB[c]	PTE[d]	II-1[e]	II-2[f]	II-3[g]
			Intramolecular H-Bond Metrics			
O···O, Å	2.554(2)	2.542(1)	2.478(4)	2.490(4)	2.554(3)	2.566(2)
O···H, Å	1.727(4)	1.703(3)	1.395(5)	1.56(1)	1.733(6)	1.759(5)
∠O−H···O, deg	147.0(2)	147.9(2)	152.1(6)	151.4(6)	147.1(3)	145.2(3)
			Covalent Bond Length Parameters			
C═O, Å	1.274(1)	1.248(1)	1.269(2)	1.265(2)	1.240(1)	1.250(1)
C−C, Å	1.456(1)	1.457(1)	1.438(2)	1.434(2)	1.466(1)	1.353(1)
C═C, Å	1.404(1)	1.404(1)	1.409(2)	1.394(3)	1.401(1)	1.405(1)
C−O, Å	1.341(1)	1.341(1)	1.317(2)	1.314(1)	1.345(1)	1.347(1)

[a] Mean Values (mv) of distances and pseudo valent angle at the H-atom with standard errors (SE). [b] All β-ketoenols in *Z*-conformation. [c] Satisfying RAHB criteria. [d] Simultaneously satisfying criteria for RAHB and PTE; belonging to the [e]II-1, [f]II-2, or [g]II-3 family.

therefore conclude that strong intramolecular H-bonding (mv 2.542(1), 1.703(3) Å, and 147.9(2)°) and marked electron density redistribution within the covalently bonded fragment (O═C−C═C−OH, mv of 1.248(1), 1.457(1), 1.404(1), 1.341(1) Å, respectively) (Table 2), are indicative of RAHB, in all types of β-ketoenols.

We then selected fragments satisfying the criteria for RAHB, with symmetric or almost symmetric positioning of the H-atoms in the six-membered pseudo-ring, ═C−O−H···O═C−C, accounting for 10% of all cases (Figure 4b). These data, indicating very strong intramolecular H-bonds (O···O and O···H distances and the pseudo valent angle at the H-atom show mv of 2.478(4), 1.395(5) Å and 152.1(6)°, respectively), together with extensive delocalization of electron density in the O═C−C═C−OH fragment (mv of 1.269(2), 1.438(2), 1.409(2), and 1.317(2) Å, respectively) demonstrate the existence of a proton translocation effect (PTE). A combination of significant conjugation and strong intramolecular hydrogen bonding is responsible for the high relative stability of such β-ketoenols.

Structural observations were classified according to the family of β-ketoenols involved. We found statistically meaningful differences between these families for intramolecular H-bonds and covalent bond parameters. The H-bond parameters indicate very strong IHB in II-1, strong IHB in II-2, and weaker IHB in II-3 (Table 2). A study of covalent bond lengths in β-ketoenol fragments showed that electron density delocalization was more marked in II-1 than in II-2 and II-3 molecules. Thus, in the almost entirely aliphatic II-1 β-ketoenols, RAHB seems to involve covalent binding between the hydrogen atom and the other two atoms involved, as originally suggested by Cleland and Kreevoy[68] and by Frey et al.[69] In molecules of the II-2 and II-3 families, IHB is weaker than that observed with molecules of the II-1 family, although still stronger than that observed with catechols. In these compounds, electron delocalization concerns not only the O═C−C═C−OH moiety but also extends to the aromatic π-systems, forming an extensive heteroconjugated network in which electronic balance give rises to nonresonant strong intramolecular hydrogen bonds.

Intermolecular H-Bonding of β-Ketoenols. It has been suggested that the hydrogen-bonded moiety of molecules stabilized by strong IHB is not involved in other hydrogen bonds.[50] However, it has also been reported that, in some structures stabilized by intramolecular H-bonding, the remaining H-donating/accepting groups remain available for intermolecular interactions.[49] We investigated the hydrogen bonding of β-ketoenols, by studying the recognition of oxygen- and nitrogen-based HBD and HBA agents. We first investigated whether the β-ketoenol moiety involved in IHB could, like catechol, form other hydrogen bonds. H-Bonding was studied for β-ketoenol acting as a donor (OH group), or as an acceptor, with the oxygen atom of the C═O or OH group serving as the acceptor center (see Figure 5).

We found that less than 15% of the β-ketoenols stabilized by IHB displayed intermolecular hydrogen bonding with HBAs, whereas 25% interacted with HBDs, using the C═O group as an acceptor and 10% interacted with HBDs, using the oxygen atom of the OH group as an acceptor. The absence of potential H-bond partners is an important but not critical reason for the absence of intermolecular H-bonds in β-ketoenols. A surprisingly large number of structures were found to have no intermolecular contacts, even if potential H-donors and H-acceptors were present. In structures containing both the β-ketoenol fragment and a potential HBD, intermolecular H-bond interactions were observed in only 40% and 20% of cases for the C═O and OH groups acting as the acceptor, respectively. Only 15% of β-ketoenols interacted as donors for hydrogen bonding, despite the presence of potential HBA groups. The stabilization of β-ketoenols in the *Z*-conformation due to strong IHB has major consequences for recognition. β-Ketoenols are extremely inefficient at H-bonding, even in the presence of potential HBD or HBA. β-Ketoenol structures are five times more common in CSD than catechols but form only a tenth as many hydrogen contacts with HBAs and a fifth as many with catechols. Like catechols, most of the partners of β-ketoenol for H-bonding are oxygen-based HBDs and HBAs.

Moderately strong intermolecular O−H···O/N H-bonds occur in only a limited number of β-ketoenols stabilized by nonresonant IHB, intermolecular H-bonding being very weak and nonlinear in structures displaying RAHB (Figure 5a,b and Table 1).

A strong negative linear correlation was found between intra- and intermolecular H-bond distances, H···O (intra) and H···O/N (inter), with an r value of −0.80. Thus, the stronger the intramolecular H-bonding is, the weaker intermolecular H-bonding is likely to be. This effect corresponds to a negative cooperativity phenomenon.[48,70] A comparison of the characteristics of intermolecular H-bonds with HBA in β-ketoenols (Figure 5a,b) and catechols (Figure 2a,b) provided further evidence that β-ketoenol does not efficiently bind HBA agents. β-Ketoenols were also found to recognize HBD agents much less efficiently than catechols, although strong, linear intermolecular H-bonds were observed in the absence of other competitive acceptor centers (Figure 5c−f, Table 1).

In parallel, we analyzed the intermolecular H-bonding of β-ketoenols from families II-1, II-2, and II-3 separately, trying to identify recognition properties specific to the molecules of these different families. We found that the recognition of HBA agents was similar for the β-ketoenols of the different families: the ratio of O−H···O/N contacts formed by the β-ketoenols of each family was consistent with the number of molecules in these families (1:5:4). The intermolecular H-bond parameters corresponded to very weak and nonlinear interactions in all β-ketoenol families (Figure 5a,b). Moderate H-bonding occurred only in molecules of the II-2 and II-3 families not displaying

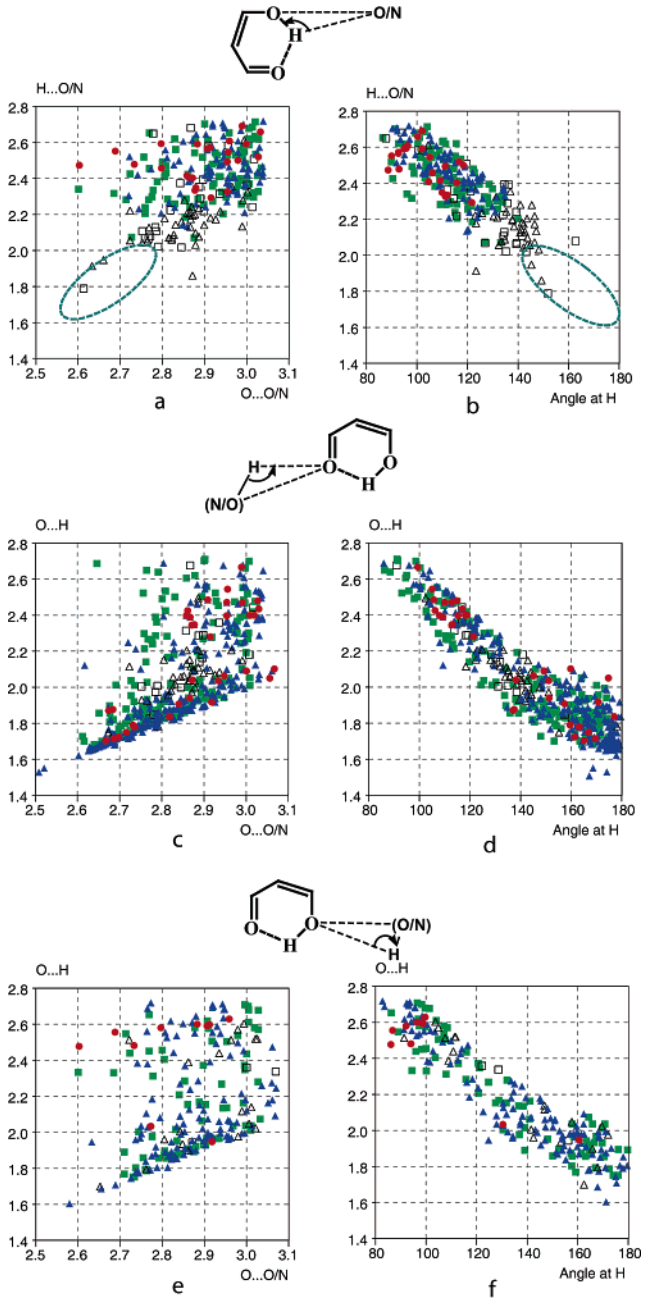

Figure 5. Intermolecular H-bonding of 2070 β-ketoenol fragments stabilized by IHB from 1524 structures. Top: β-ketoenol acts as a donor in 215 structures forming 275 O−H···O/N contacts. Scatter plot of **(a)** O···O/N vs H···O/N and **(b)** H···O/N vs pseudo valent angle at the H-atom. Middle: β-ketoenol acts as an acceptor (C═O) in 365 structures forming 474 O···H−(O/N) contacts. Scatter plots of **(c)** O···O/N vs O···H and (d) O···H vs pseudo valent angle at the H-atom. Bottom: β-ketoenol acts as an acceptor (OH) in 175 structures forming 215 O···H−(O/N) contacts. Scatter plots of **(e)** O···O/N vs O···H and **(f)** O···H vs pseudo valent angle at the H-atom. The experimentally determined H-atom positions were used for the analysis of O−H···O/N interactions and were normalized in the analysis of O···H−(O/N) interactions. Intramolecular hydrogen bonds satisfying RAHB criteria (O···O ≤ 2.70, O···H ≤ 2.0) are indicated as full symbols, red circles for (II-1), blue triangles for (II-2), and green squares for (II-3). Intramolecular hydrogen bonds with bond distances shorter than the sum of Van der Waals radii but longer than RAHB criteria are shown as open symbols ○ for (II-1), △ for (II-2), and □ for (II-3). Domains encircled by broken lines indicate the areas most populated by catechols.

RAHB and was never observed in molecules from the II-1 family. β-Ketoenols from different families also differed slightly in their recognition of HBD agents. O···H−(O/N) H-bonds occurred with a frequency ratio of 1:9:5 for the II-1, II-2, and II-3 families, respectively, for both acceptor centers: C═O and OH. Given the ratio for the numbers of molecules belonging to these families (1:5:4), this suggests that O···H−(O/N) H-bonds are formed significantly more frequently in molecules of the II-2 family. Intermolecular H-bond parameters indicated that the strength of HBD interactions with the C═O acceptor center was almost identical in all families, whereas interactions with the OH acceptor center were much more linear and stronger in β-ketoenols of the II-2 and II-3 families than in those of the II-1 family (Figure 5c−f). These subtle differences may lead to divergence in the pharmacological properties of molecules from the II-1, II-2, and II-3 families.

Coordination to Magnesium and Manganese. The integrase of HIV-1, which belongs to a large family of polynucleotidyl transferases, requires Mn or Mg for activity *in vitro*.[71−73] Mg^{2+} is the most likely cofactor *in vivo*.[25,74] As the conformation of the active site of the HIV-1 integrase may differ according to whether it contains Mn^{2+} or Mg^{2+}, the mode of interaction between inhibitors and ion-loaded active sites may vary. We focus here on the interaction of catechol and β-ketoenol with Mg and Mn, and the specificity of binding of these interactions. Both ligands are bidentate and bind metals avidly either *via* a single atom or through chelation. Chelation gives more stable complexes and is therefore the only mode of coordination considered here. We included all crystal structures of Mg and Mn complexes, identified by coordination number and oxidation state, in the statistical analysis. Given the specificity of the interactions of β-ketoenol and catechol with metals (complexes characterized by valence tautomerism or "resonant forms"[75−77]), the terms "β-ketoenolate" and "dioxolene", and the abbreviations L1 and L2 will be used hereafter.

General Observations. Mn and Mg are found in only a few of the many structures involving metals chelated with L1 (2488 entries) and L2 (1172 entries): only about 7% of β-ketoenolates and 5% of dioxolenes display Mn or Mg chelation. Mn and Mg complexes are five times more common in β-ketoenolates than in dioxolenes. Most M−L1 complexes (97%) are hexacoordinated, and Mn complexes predominate (Mg:Mn ratio of 1:3). The ratio of the two metals was similar for pentacoordinated complexes. Hexacoordinated complexes account for 75%, and pentacoordinated complexes 25% of M−L2 complexes. Mn strongly predominates in these complexes, with an Mg:Mn ratio of 1:15 in hexacoordinated complexes and of 1:7 in pentacoordinated complexes. Heptacoordination was observed in only a few M−L2 complexes. We included the small number of penta- and heptacoordinated complexes in subsequent analysis but not in our interpretation.

Coordination Geometry of the M−L1 Moiety. M···O coordination bond distances in M−L1 complexes formed three dense clusters on the scatter plot (Figure 6a), corresponding to MnIII/MnIV (MnIII and MnIV complexes considered together), MgII, and MnII. M···O bond distances were almost symmetric in Mn complexes, with mv of 1.909(2) and 2.150(2) Å for MnIII/MnIV and MnII, respectively, and slightly asymmetric in MgII complexes, with slightly different mv of 2.036(2) and 2.052(2) Å (Table 3). The mean Mn^{2+}···O distance was about 0.11 Å longer than the mean Mg^{2+}···O distance, consistent with the larger ionic radius of Mn^{2+} (0.74 Å) than of Mg^{2+} (0.65 Å). The marked difference in Mn···O bond distances (>0.24 Å) between MnII and MnIII/MnIV complexes illustrates the strong influence of Mn oxidation state on the coordination bond: the higher the oxidation number of the metal ion, the closer the atoms of the ligand. The O···M···O coordination was

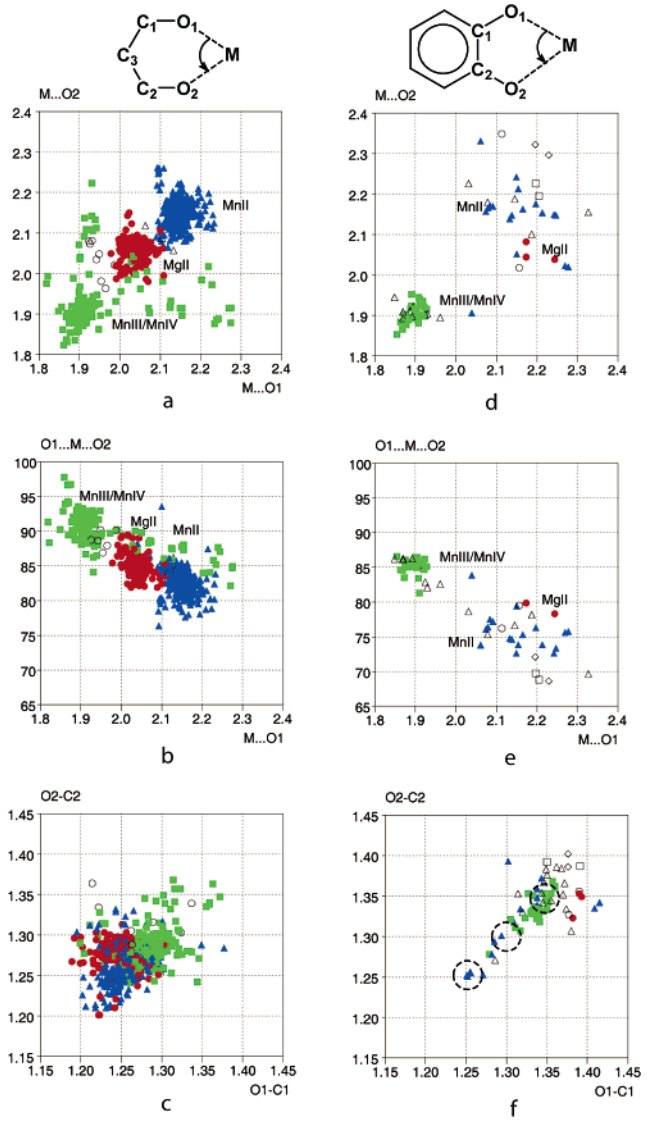

Figure 6. Ligand interactions with Mg and Mn. Left: Coordination geometry of β-ketoenolate complexes observed in 561 M−L1 fragments from 224 structures. Scatter plots of **(a)** M···O1 vs M···O2, **(b)** M···O1 vs O1···M···O2, **(c)** O1−C1 vs O2−C2. Right: Coordination geometry of dioxolene complexes observed in 105 M−L2 fragments from 45 structures. Scatter plots of **(d)** M···O1 vs M-O2, **(e)** M···O1 vs O1···M···O2, **(f)** O1−C1 vs O2−C2. Hexacoordinated complexes are indicated by full symbols: red circles (MgII), blue triangle (MnII), and green squares (MnIII, IV). Penta- and heptacoordinated complexes are indicated by open symbols: △ (Mn, 5), □ (Mg, 7), ◇ (Mn, 7). Oxidation states of metals are indicated; domains encircled by broken lines show C−O values typical of the catechol, semiquinone, and quinone forms of M−L2.

strongly correlated with M···O distance (*r* of −0.87). Three distinct clusters were identified, corresponding to MnIII/MnIV, MgII, and MnII complexes with mv of 90.8(2), 84.9(2), and 82.9(2)°, respectively (Figure 6b; Table 3). The O···Mg^{2+}···O coordination angle is slightly larger than that for O···Mn^{2+}···O, suggesting that the coordination of Mg^{2+} may be less strained than that of Mn^{2+}. The coordination angle characterizing divalent Mn is larger than that for MnIII/MnIV by 8−10°. Thus, the coordination geometry of M−L1 complexes is determined by the nature of the metal, its size (Mg or Mn), and oxidation state (MnII or MnIII/IV).

The C−O and C−C bond distances of ligand L1 also seem to depend on the nature of the metal. Thus, in Mg complexes, the chemically related distances of the ligand are asymmetric (mv of 1.241(2) and 1.276(1) Å for O−C distances and of 1.389(3) and 1.425(3) Å for C−C distances), whereas the geometry of the ligand is perfectly symmetric in Mn complexes, but with differences observed between MnII and MnIII/IV complexes (Figure 6c). C−O bond distances are shorter in MnII (mv of 1.252(1) Å) than in MnIII/IV (mv of 1.293(2) Å). C−C bond distances are almost identical in MnII (mv of 1.395(1) Å) and MnIII/IV complexes (mv of 1.404(4) Å). No correlations were found between M···O, C−O, and C−O bond distances. These structural data were found to be correlated with thermodynamic parameters: standard enthalpies of formation of the crystalline metal complexes, $\Delta H°_f$(c), and the calculated mean of metal−oxygen bond-dissociation enthalpies <D>(M−O), reported for Mg and Mn chelated with a series of β-ketoenolates (Table 3).[78]

Coordination Geometry of the M−L2 Moiety. The M···O bond distances in M−L2 complexes were almost symmetric (*r* of 0.81), as for M−L1 complexes. However, only one single dense cluster was distinguished with a mv of 1.898(3) Å (Figure 6d; Table 3). This cluster included most of the data and corresponded to MnIII and MnIV complexes, which were considered together. The other points formed a diffuse cloud corresponding to MgII and MnII complexes. The M···O distances in Mg−L2 complexes appears to be asymmetric (mv of 2.05(1) and 2.20(1) Å), whereas those in MnII complexes were almost symmetric (mv of 2.16(1) Å), although too few data are available for firm conclusions to be drawn. The coordination angle formed by the metal and the two oxygen atoms of L2, O···M···O, was strongly correlated with M···O distances (*r* of −0.90) (Figure 6e). This angle was 10° smaller in MgII and MnII complexes than in MnIII/MnIV complexes (mv of 85.1(1)°). Thus, based on an analysis of limited structural data, the coordination geometry of M−L2 seems to depend strongly on oxidation state (MnII or MnIII/MnIV) but not metal size.

In Mn complexes, O−C bond distances were symmetric (*r* of 0.74), ranging from 1.25 to 1.42 Å, whereas they were probably asymmetric in Mg complexes (mv of 1.345(6) and 1.390(2) Å) (Figure 6f). Many structural inter-relationships were observed in M−L2 fragments, in contrast to M−L1 complexes. O−C bond distances were correlated with adjacent C−C bonds (*r* of −0.85), and M···O distances were correlated with both the angle at the metal and with the angles at the oxygen atoms of L2 (*r* of 0.73).

Comparison of M−L1 and M−L2 Binding. Limited structural data on dioxolenes make it difficult to draw firm conclusions. Mn and Mg complexes chelated with β-ketoenolates were five times more common than those chelated with dioxolenes, suggesting that β-ketoenolate was a much more effective chelating ligand for these metals. Alternatively, this difference may be due to a bias toward structural studies of M−L1 rather than M−L2 complexes.

β-Ketoenolate appears to display preferential binding to Mn, as Mn complexes accounted for 75% of all M−L1 chelates. However, if the oxidation state of Mn was taken into account, we found that there were similar numbers of divalent Mg and divalent Mn complexes. Conversely, only 5% of M−L2 complexes included the Mg cation, the rest being complexed with Mn. If divalent cations were compared, Mg chelates accounted for 15% and Mn chelates 85% of complexes, reflecting the high selectivity of dioxolenes for Mn^{2+} cation.

Mn and Mg are chelated by polar σ-donor groups, hydroxyl and/or carbonyl in nature, with two oxygen-coordinating heteroatoms. This results in different structural arrangements of

Table 3. Binding of b-Ketoenolate (M−L1) and Dioxolene (M−L2) Complexes [M = metal (Mg, Mn)][a]

	M−L1			M−L2		
metal	M···O, Å	O···M···O, deg	$\Delta H°_f$(c), kJ mol^{-1}	M···O, Å	O···M···O, deg	radii, Å
MgII	2.036 (2)	84.9(2)	−1263	2.05(1)	78.5(1)	2.07/2.18
	2.052 (2)			2.20(1)		
MnII	2.150(2)	82.9(2)	−1048	2.16(1)	75.5(1)	2.1/2.1
MnIII/MnIV	1.909(2)	90.8(2)	−1379	1.898(3)	85.1(1)	1.96/2.1

[a] Mean values (mv) of M···O distances and O···M···O angles with standard errors (SE), standard enthalpies of M−L1 formation, $\Delta H°_f$(c),[78] and sum of ionic/covalent radii.[75]

the chelated cycles, a six-membered cycle in M−L1 structures and a five-membered ring in M−L2 complexes. Steric constraints in five-membered M−L2 complexes result in more cramped coordination angles at the metal than in unstressed six-membered M−L1 chelates. The M···O coordination bonds were almost symmetric and identical in Mn−L1 and Mn−L2 complexes formed by Mn cations of the same oxidation state, whereas the Mg···O bond tended to be slightly asymmetric in M−L1 and asymmetric in M−L2. Ligand L1 chelated to the MgII ion displayed mostly localized covalent bonds in the O═C−C−C═C−O fragment and would therefore be more appropriately described as a ketoenolate form. Most of the MnII−L1 complexes had similar symmetry-related O−C and C−C bond distances corresponding to a diketonate form. The MnIII/IV-chelated ligand L1 showed partial or complete electron density delocalization and therefore corresponded to an anionic "enolate" form.

On the basis purely of these structural data (number of observations and the value of coordination bond lengths), we can conclude that β-ketoenolates are not selective ligands of MgII and MnII cations. However, taking into account the tautomeric forms of β-ketoenolate (diketone, ketoenol, and anionic enolate), we identified different roles for metal cations: MgII preferentially bound to β-ketoenol molecules whereas MnII preferentially bound the diketo form.

The reported structures of Mn and Mg, with the same β-ketoenol-based ligand, are extremely rare in CSD. Nonetheless, complexes of norfloxacin with MgII (TAFJUC) and MnII (XAVKUA) are of particular interest, as they are representative of this selectivity, with Mg binding the β-ketoenol form and Mn binding the diketo form of norfloxacin. The oxygen−carbon bond distances in the ligand were non-equivalent (1.256 Å and 1.283 Å) in the Mg complex and correspond better to localized double C═O and single C−O bonds, whereas identical values were obtained for oxygen−carbon bonds in Mn complexes (1.263 Å), both such bonds showing a double bond character.

Experimental studies have shown that the various quinoid forms of dioxolene are characterized by typical C−O bond distances: 1.35 Å in catechol, 1.30 Å in semiquinone, and 1.25 Å in quinone.[77,79] The structural data analyzed here indicated that MnII complexes were formed by all types of dioxolene, whereas most of the MnIII/IV complexes formed involved catecholates (Figure 6f). C−O bond distance (mv of 1.37(4) Å) in Mg−L2 complexes is identical to that in the isolated catechol molecule, indicating a pure catecholate form for all Mg−L2 chelates.

Thus, the geometry of M−L1 and M−L2 fragments therefore reflect a subtle balance of electronic effects between the two partners, the ligand and the metal. Cation binding probably affects the state of the ligand.

Binding Mode Selectivity of Catechols and β-Ketoenols. We have described the structural and recognition properties of catechol and β-ketoenol with respect to both divalent metals, Mg and Mn, and to HBDs and HBAs. Our three-dimensional, structure-based, *in silico*-driven approach is the first systematic and comparative study of two important, widely used pharmacophores and was designed as the basis for fragment-based drug design discovery and the optimization of HIV-1 IN inhibitors. The importance of catechol and β-ketoenols as pharmacophores is clear from the large number of drugs containing these fragments. The structures of some of these molecules have been determined and deposited in the CSD.[42] About 30% of all catechols and 20% of all β-ketoenols in the CSD are reported to have biological activity (classified as "drug", "inhibitor", "agent", or "active"). Hydrogen bonding is a key factor for the selectivity of protein−ligand interactions. The number of hydrogen bonds formed between protein and ligand has been reported to vary between 0 and 11.[80] We analyzed the structures containing both catechol and β-ketoenol: 17 molecules of the 67 (25%) molecules containing both pharmacores were reported to be active. These molecules had diverse biological activities and recognition patterns. WUXGIF (pormiferin, antifungal activity) was found to have multiple intermolecular H-bonds formed by catechol alone. In RAMGOB (baicalein, various activities, including anti-HIV-1), four of the six H-bonds are formed by catechol and two by β-ketoenol. Macluraxanthone B (FOLWAE) and cudraxanthone L (FOLWEJ) are of particular interest as they are regioisomers with cytotoxic activity against human cancer cell lines. The pharmacophores of both structures are stabilized by intramolecular H-bonding, but these molecules have different intermolecular recognition patterns. In FOLWAE, each pharmacophore forms only a single H-bond, whereas in FOLWEJ, the catechol is encircled by multiple environmental HBD and HBA agents and forms five H-bonds.

Some pharmacological projects have attempted to incorporate two or more pharmacophores into a single molecule with the aim of designing multipotent agents with more than one target in HIV-1 IN. Catechols and β-ketoenols can inhibit multiple targets in HIV-1 IN, but the extent to which multiple pharmacological effects can be combined into a single molecule remains unclear. We show here that statistical analyses of structural data can predict recognition between partners. The catechol group displayed an outstanding ability to recognize both HBD and HBA simultaneously, forming multiple H-bonds, although it bound less strongly to HBD than to HBA. We also characterized the recognition and affinity of catechol as a function of its conformation (*E*,*E*-, *Z*,*E*-, and *Z*,*Z*-catechols). We found that the intramolecular H-bond (IHB) in *Z*,*E*-catechols was too weak to prevent the recognition of HBA and HBD agents, leading to the formation of multiple, strong intermolecular interactions. IHB nonetheless affected the nature of the interaction of *E*- and *Z*-hydroxyl groups with their partners and the strength of intermolecular H-bonding. Unlike catechol, the β-ketoenol moiety is stabilized by very strong IHB. Due to this IHB, β-ketoenol cannot bind HBA strongly and has a much lower capacity for interacting with HBD than catechol. This lower ability of β-ketoenols to interact with HBD and the absence of

strong and directed H-bond interactions with HBA result from two intramolecular effects: RAHB and, in some cases, PTE.

The structural data indicate that there are significant differences in the selectivity of dioxolene and β-ketoenolate, accounting for differences in the behavior of the two types of inhibitor in the presence of Mg^{2+} or Mn^{2+} *in vitro*. β-Ketoenolate chelated both divalent metals more efficiently than dioxolene, which displayed a clear preference for the Mn cation. These data are consistent with experimental data on HIV-1 IN inhibition. Indeed, this effect may account for catechol-containing inhibitors being identified mostly in *in vitro* assays of the Mn-dependent activity of IN. In contrast, ketoenolate-containing inhibitors were identified when IN activity was tested in the presence of Mg.

Taking into account the tautomeric forms of β-ketoenolates, different roles were identified for the metal cations: Mg^{2+} seems to bind preferentially to β-ketoenol molecules whereas Mn^{2+} binds predominantly to the diketo form. Mg^{2+} is believed to be the physiological cofactor, so ketoenol is probably the most active tautomeric form of such inhibitors. The stabilization of such forms may increase their inhibitory activity.

We compared the reported modes of binding of compounds containing either a catechol group or both catechol and β-ketoenol fragments, using a docking approach based on a crystallographic model. It has been reported that the most favorable interaction involves metal chelation by the hydroxyquinoline moiety, with catechol involved in noncovalent recognition, π-stacking, or H-bonding,[31,32,81] consistent with our predictions.

Conclusions

We analyzed two crucial aspects of catechol and β-ketoenol recognition: their binding to the divalent metals, Mg and Mn, which serve as the cationic cofactors for HIV-1 integrase, and to HBD and HBA, corresponding to probes for hydrophilic amino acids. We studied the structural and recognition properties of these structures, using data retrieved from the Cambridge Structural Database (CSD).

We found that most catechols (65%) and the vast majority of β-ketoenols (96%) were stabilized by intramolecular H-bonding, which was weak in *Z,E*-catechols and very strong in *Z*-β-ketoenols. All conformations of catechols (*E,E*, *E,Z*, and *Z,Z*) tended to recognize environmental HBDs and HBAs, demonstrating their ability to make use of both hydroxyl groups to form multiple, strong intermolecular H-bonds. In contrast, β-ketoenols stabilized in the *Z*-conformation by strong IHB formed H-bonds with HBAs and HBDs only inefficiently.

β-Ketoenolate chelated both Mg and Mn ions much more efficiently than dioxolene, which was highly selective for Mn cations. We identified different roles for the metal cations: MgII bound preferentially to the β-ketoenol form of β-ketoenolate, whereas MnII bound predominantly to the diketo form.

Both catechol and ketoenol have been considered to be anti-IN metal-chelating pharmacophores. Our study, reporting specificities in the recognition properties of β-ketoenol and catechol, suggests that these two pharmacophores make very different contributions to the action of anti-integrase drugs and that these differences should be taken into account in the development and improvement of inhibitors by fragment-based design.

Methods

Database Searches. Relevant structures were retrieved from the Cambridge Structural Database (CSD, 2006 Release, 366 886 entries).[42] Substructural searches, geometry calculations, and data analyses were carried out with the CSD programs ConQuest 1.8,[82] Vista.[83] Structures flagged in the database as being erroneous or disordered or as containing polymeric connections were rejected from the analysis. PC Microsoft Windows XP and PC Linux Fedora 4.0 computers were used for all calculations.

Structure. We investigated the conformation, molecular geometry, and intramolecular H-bonding of two groups of molecules: one based on catechol (I) and the other on β-ketoenol (II) fragments (Chart 1). The molecules based on β-ketoenol were classified into three families as a function of the nature of the carbon atoms (cyclic or acyclic): (II-1), aliphatic β-ketoenols, in which all carbon atoms were acyclic; (II-2) α-acylphenyl derivatives, in which the carbonyl atom was acyclic and the other two were cyclic; (II-3) β-ketoenol-like fragments in which all the carbon atoms were cyclic and inserted into bicyclic rings. The structures used as examples are referenced, together with their CSD refcodes.

Hydrogen Bonding. The intermolecular H-bonding of (I) and (II) with HBD, where D = O/N, and HBA, where A = O/N, was investigated for crystal structures containing both the studied fragment and HBD or HBA agents. Generic target-probe interactions with the hydrogen held either by the target or by the probe are shown in Figure 2 for (I) and in Figure 5 for (II). Definition of parameters: O···O/N is the distance between donor and acceptor atoms; H···O/N and O···H are distances between the H-atom and acceptor and ∠O−H···O/N or ∠O···H(O/N) is the pseudo valent angle at the H-atom. Intermolecular contacts less than sum of van der Waals radii were calculated for the independent fragments. We characterized the number of contacts on an atom (i.e the atom environment) by taking into account symmetry-related fragments. The H-atoms involved in nonbonded contact searches were placed in normalized positions,[82] except in one study on intramolecular H-bonds in (II), in which experimental H-atom positions were used. The H-atom position in (II) was considered to be symmetric or almost symmetric for intramolecular H-bonds, with $\Delta = \text{abs}[d(\text{O}\cdots\text{H}) - d(\text{O}-\text{H})] \leq 0.4$ Å.

Metal−Ligand Interactions. The coordination geometry was probed for all Mn and Mg complexes chelated with ketoenolate (L1) and dioxolene (L2) ligands, as indicated in Figure 6. As it was difficult to determine the nature of the bond, this search was carried out for generalized fragments in which (i) L1 or L2 was coordinated in a bidentate fashion to the metal (M═Mn and Mg), (ii) the M−O bond was any type, (iii) each O-atom could have only two bonds, (iv) the O−C and C−C bonds could be single, double or intermediate, (v) atomic charges were not specified, and (vi) all derivatives of the ligands were considered. The metals were classified according to type (Mg or Mn), and metal coordination was considered within data subsets. The resulting subset was investigated manually, and all entries were sorted according to Mn oxidation state. The oxidation state specified in the compound name field was used as a primary criterion. In structures with non-reported metal charges, oxidation state had to be checked by a detailed inspection of molecular structure. If there was any doubt as to the correct assignment of oxidation state, the structure was excluded from further analysis. No other restrictions were imposed in our data analysis.

Structural Analysis. A simple and general computational procedure was carried out with all selected crystallographic observations. For each instance of each fragment, the related geometric parameters (torsion angles, bond distances, bond angles, non-bonded contacts, and pseudo valent angles at H- and O-atoms) were calculated. Once all the information had been accumulated, we obtained a data matrix of dimension $m \times n$, where m is the number of calculated parameters and n is the number of fragments counted. Matrices were analyzed using various graphical, statistical, and numerical techniques. We estimated relationships in molecular fragments I and II, and in their complexes M−L1 and M−L2, by carrying out univariate and bivariate analysis. The results obtained for univariate analysis are presented as numerical values, and those for bivariate analyses are presented as scatter plots. Statistical descriptors are as defined by Snedocor and Cochran.[44] Individual molecular structures were viewed with Mercury 1.4.1.[84] Donor and

acceptor surfaces of nonsubstituted catechols were reovered from high-resolution crystal structures (FIBMUY (*E*,*E*), CATCOL13 (*Z*,*E*), and DEWFUG (*Z*,*Z*)) and viewed with Benchware 3D Explorer.[56]

Acknowledgment. We thank Dr. Alex Yanovsky and Prof. Nour Eddine Ghermani for valuable intellectual input and discussions throughout this project and Dr. Phillipe Cotelle for critical reading of the manuscript. J.-F. Mouscadet's team is funded by the French Centre National pour la Recherche Scientifique (CNRS). This work was supported by the TRIoH European project (FP6 grant 503480).

References

(1) Ellison, V.; Gerton, J.; Vincent, K. A.; Brown, P. O. An essential interaction between distinct domains of HIV-1 integrase mediates assembly of the active multimer. *J. Biol. Chem.* **1995**, *270*, 3320−3326.

(2) Zheng, R.; Jenkins, T. M.; Craigie, R. Zinc folds the N-terminal domain of HIV-1 integrase, promotes multimerization, and enhances catalytic activity. *Proc. Natl. Acad. Sci. U.S.A.* **1996**, *93*, 13659−13664.

(3) Dyda, F.; Hickman, A. B.; Jenkins, T. M.; Engelman, A.; Craigie, R.; Davies, D. R. Crystal structure of the catalytic domain of HIV-1 integrase: similarity to other polynucleotidyl transferases. *Science* **1994**, *266*, 1981−1986.

(4) Engelman, A.; Bushman, F. D.; Craigie, R. Identification of discrete functional domains of HIV-1 integrase and their organization within an active multimeric complex. *EMBO J.* **1993**, *12*, 3269−3275.

(5) Wlodawer, A. Crystal structures of catalytic core domains of retroviral integrases and role of divalent cations in enzymatic activity. *Adv. Virus Res.* **1999**, *52*, 335−350.

(6) Esposito, D.; Craigie, R. Sequence specificity of viral end DNA binding by HIV-1 integrase reveals critical regions for protein-DNA interaction. *EMBO J.* **1998**, *17*, 5832−5843.

(7) Gao, K.; Butler, S. L.; Bushman, F. Human immunodeficiency virus type 1 integrase: arrangement of protein domains in active cDNA complexes. *EMBO J.* **2001**, *20*, 3565−3576.

(8) Lutzke, R. A.; Vink, C.; Plasterk, R. H. Characterization of the minimal DNA-binding domain of the HIV integrase protein. Formation of a stable complex between the human immunodeficiency virus integrase protein and viral DNA. *Nucleic Acids Res.* **1994**, *22*, 4125−4131.

(9) Lutzke, R. A.; Plasterk, R. H. Structure-based mutational analysis of the C-terminal DNA-binding domain of human immunodeficiency virus type 1 integrase: critical residues for protein oligomerization and DNA binding. *J. Virol.* **1998**, *72*, 4841−4848.

(10) Craigie, R. HIV integrase, a brief overview from chemistry to therapeutics. *J. Biol. Chem.* **2001**, *276*, 23213−23216.

(11) Dayam, R.; Deng, J.; Neamati, N. HIV-1 integrase inhibitors: 2003−2004 update. *Med. Res. Rev.* **2006**, *26*, 271−309.

(12) Garcia-Gasco, P.; Blanco, F.; Soriano, V. Integrase inhibitors. *J. HIV Ther.* **2005**, *10*, 75−78.

(13) Johnson, A. A.; Marchand, C.; Pommier, Y. HIV-1 integrase inhibitors: a decade of research and two drugs in clinical trial. *Curr. Top. Med. Chem.* **2004**, *4*, 1059−1077.

(14) Burke, T. R., Jr.; Fesen, M. R.; Mazumder, A.; Wang, J.; Carothers, A. M.; Grunberger, D.; Driscoll, J.; Kohn, K.; Pommier, Y. Hydroxylated aromatic inhibitors of HIV-1 integrase. *J. Med. Chem.* **1995**, *38*, 4171−4178.

(15) Cushman, M.; Golebiewski, W. M.; Pommier, Y.; Mazumder, A.; Reymen, D.; De Clercq, E.; Graham, L.; Rice, W. G. Cosalane analogues with enhanced potencies as inhibitors of HIV-1 protease and integrase. *J. Med. Chem.* **1995**, *38*, 443−452.

(16) Fesen, M. R.; Pommier, Y.; Leteurtre, F.; Hiroguchi, S.; Yung, J.; Kohn, K. W. Inhibition of HIV-1 integrase by flavones, caffeic acid phenethyl ester (CAPE) and related compounds. *Biochem. Pharmacol.* **1994**, *48*, 595−608.

(17) Dupont, R.; Jeanson, L.; Mouscadet, J. F.; Cotelle, P. Synthesis and HIV-1 integrase inhibitory activities of catechol and bis-catechol derivatives. *Bioorg. Med. Chem. Lett.* **2001**, *11*, 3175−3178.

(18) Espeseth, A. S.; Felock, P.; Wolfe, A.; Witmer, M.; Grobler, J.; Anthony, N.; Egbertson, M.; Melamed, J. Y.; Young, S.; Hamill, T.; Cole, J. L.; Hazuda, D. J. HIV-1 integrase inhibitors that compete with the target DNA substrate define a unique strand transfer conformation for integrase. *Proc. Natl. Acad. Sci. U.S.A.* **2000**, *97*, 11244−11249.

(19) Goldgur, Y.; Craigie, R.; Cohen, G. H.; Fujiwara, T.; Yoshinaga, T.; Fujishita, T.; Sugimoto, H.; Endo, T.; Murai, H.; Davies, D. R. Structure of the HIV-1 integrase catalytic domain complexed with an inhibitor: a platform for antiviral drug design. *Proc. Natl. Acad. Sci. U.S.A.* **1999**, *96*, 13040−13043.

(20) Hazuda, D. J.; Felock, P. J.; Witmer, M. V.; Wolfe, A.; Stillmock, K. A.; Grobler, J.; Espeseth, A. S.; Gabryelski, L.; Schleif, W. A.; Blau, C.; Miller, M. D. Inhibitors of strand transfer that prevent integration and inhibit HIV-1. *Science* **2000**, *287*, 646−650.

(21) Hazuda, D. J.; Anthony, N. J.; Gomez, R. P.; Jolly, S. M.; Wai, J. S.; Zhuang, L.; Fisher, T. E.; Embrey, M.; Guare, J. P., Jr.; Egbertson, M. S.; Vacca, J. P.; Huff, J. R.; Felock, P. J.; Witmer, M. V.; Stillmock, K. A.; Danovich, R.; Grobler, J.; Miller, M. D.; Espeseth, A. S.; Jin, L.; Chen, I. W.; Lin, J. H.; Kassahun, K.; Ellis, J. D.; Wong, B. K.; Xu, W.; Pearson, P. G.; Schleif, W. A.; Cortese, R.; Emini, E.; Summa, V.; Holloway, M. K.; Young, S. D. A naphthyridine carboxamide provides evidence for discordant resistance between mechanistically identical inhibitors of HIV-1 integrase. *Proc. Natl. Acad. Sci. U.S.A.* **2004**, *101*, 11233−11238.

(22) Grobler, J. A.; Stillmock, K.; Hu, B.; Witmer, M.; Felock, P.; Espeseth, A. S.; Wolfe, A.; Egbertson, M.; Bourgeois, M.; Melamed, J.; Wai, J. S.; Young, S.; Vacca, J.; Hazuda, D. J. Diketo acid inhibitor mechanism and HIV-1 integrase: implications for metal binding in the active site of phosphotransferase enzymes. *Proc. Natl. Acad. Sci. U.S.A.* **2002**, *99*, 6661−6666.

(23) Long, Y. Q.; Jiang, X. H.; Dayam, R.; Sanchez, T.; Shoemaker, R.; Sei, S.; Neamati, N. Rational design and synthesis of novel dimeric diketoacid-containing inhibitors of HIV-1 integrase: implication for binding to two metal ions on the active site of integrase. *J. Med. Chem.* **2004**, *47*, 2561−2573.

(24) Marchand, C.; Johnson, A. A.; Karki, R. G.; Pais, G. C.; Zhang, X.; Cowansage, K.; Patel, T. A.; Nicklaus, M. C.; Burke, T. R., Jr.; Pommier, Y. Metal-dependent inhibition of HIV-1 integrase by beta-diketo acids and resistance of the soluble double-mutant (F185K/C280S). *Mol. Pharmacol.* **2003**, *64*, 600−609.

(25) Neamati, N.; Lin, Z.; Karki, R. G.; Orr, A.; Cowansage, K.; Strumberg, D.; Pais, G. C.; Voigt, J. H.; Nicklaus, M. C.; Winslow, H. E.; Zhao, H.; Turpin, J. A.; Yi, J.; Skalka, A. M.; Burke, T. R., Jr.; Pommier, Y. Metal-dependent inhibition of HIV-1 integrase. *J. Med. Chem.* **2002**, *45*, 5661−5670.

(26) Brigo, A.; Lee, K. W.; Fogolari, F.; Mustata, G. I.; Briggs, J. M. Comparative molecular dynamics simulations of HIV-1 integrase and the T66I/M154I mutant: binding modes and drug resistance to a diketo acid inhibitor. *Proteins* **2005**, *59*, 723−741.

(27) Brigo, A.; Mustata, G. I.; Briggs, J. M.; Moro, S. Discovery of HIV-1 integrase inhibitors through a novel combination of ligand and structure-based drug design. *Med. Chem.* **2005**, *1*, 263−275.

(28) Chen, I. J.; Neamati, N.; MacKerell, A. D., Jr. Structure-based inhibitor design targeting HIV-1 integrase. *Curr. Drug Targets* **2002**, *2*, 217−234.

(29) Dayam, R.; Neamati, N. Active site binding modes of the beta-diketoacids: a multi-active site approach in HIV-1 integrase inhibitor design. *Bioorg. Med. Chem.* **2004**, *12*, 6371−6381.

(30) Dayam, R.; Sanchez, T.; Clement, O.; Shoemaker, R.; Sei, S.; Neamati, N. Beta-diketo acid pharmacophore hypothesis. 1. Discovery of a novel class of HIV-1 integrase inhibitors. *J. Med. Chem.* **2005**, *48*, 111−120.

(31) Deprez, E.; Barbe, S.; Kolaski, M.; Leh, H.; Zouhiri, F.; Auclair, C.; Brochon, J. C.; Le Bret, M.; Mouscadet, J. F. Mechanism of HIV-1 integrase inhibition by styrylquinoline derivatives in vitro. *Mol. Pharmacol.* **2004**, *65*, 85−98.

(32) Ma, X.; Zhang, X.; Tan, J.; Chen, W.; Wang, C. Exploring binding mode for styrylquinoline HIV-1 integrase inhibitors using comparative molecular field analysis and docking studies. *Acta Pharmacol. Sin.* **2004**, *25*, 950−958.

(33) Maurin, C.; Bailly, F.; Cotelle, P. Structure-activity relationships of HIV-1 integrase inhibitors−enzyme-ligand interactions. *Curr. Med. Chem.* **2003**, *10*, 1795−810.

(34) Rao, G. S.; Bhatnagar, S.; Ahuja, V. Structure-based design of a novel peptide inhibitor of HIV-1 integrase: a computer modeling approach. *J. Biomol. Struct. Dyn.* **2002**, *20*, 31−38.

(35) Sotriffer, C. A.; Ni, H.; McCammon, J. A. Active site binding modes of HIV-1 integrase inhibitors. *J. Med. Chem.* **2000**, *43*, 4109−4117.

(36) Karki, R. G.; Tang, Y.; Burke, T. R., Jr.; Nicklaus, M. C. Model of full-length HIV-1 integrase complexed with viral DNA as template for anti-HIV drug design. *J. Comput.-Aided Mol. Des.* **2004**, *18*, 739−760.

(37) Maurin, C.; Bailly, F.; Mbemba, G.; Mouscadet, J. F.; Cotelle, P. Design, synthesis, and anti-integrase activity of catechol-DKA hybrids. *Bioorg. Med. Chem.* **2006**, *14*, 2978−2984.

(38) Mekouar, K.; Mouscadet, J. F.; Desmaele, D.; Subra, F.; Leh, H.; Savoure, D.; Auclair, C.; d'Angelo, J. Styrylquinoline derivatives: a new class of potent HIV-1 integrase inhibitors that block HIV-1 replication in CEM cells. *J. Med. Chem.* **1998**, *41*, 2846−2857.
(39) Zouhiri, F.; Mouscadet, J. F.; Mekouar, K.; Desmaele, D.; Savoure, D.; Leh, H.; Subra, F.; Le Bret, M.; Auclair, C.; d'Angelo, J. Structure-activity relationships and binding mode of styrylquinolines as potent inhibitors of HIV-1 integrase and replication of HIV-1 in cell culture. *J. Med. Chem.* **2000**, *43*, 1533−1540.
(40) Böhm, H.-J.; Brode, S.; Hesse, U.; Klebe, G. Oxygen and Nitrogen in Competitive Situations: Which is the Hydrogen-Bond Acceptor? *Chem.−Eur. J.* **1996**, *2*, 1509−1513.
(41) Gohlke, H. K. G. Approaches to the Description and Prediction of the Binding Affinity of Small-Molecule Ligands to Macromolecular Receptors. *Angew. Chem., Int. Ed.* **2002**, *41*, 2644−2676.
(42) Allen, F. H. The Cambridge Structural Database: a quarter of a million crystal structures and rising. *Acta Crystallogr. B* **2002**, *58*, 380−388.
(43) Taylor, R. Life Science applications of the Cambridge Structural Database. *Acta Crystallogr. D* **2002**, *58*, 879−888.
(44) Snedecor, G. W.; Cochran, W. G. *Statistical Methods*; Iowa State University Press: Ames, Iowa, 1989; p 503.
(45) Konschin, H. An STO-3G molecular orbital investigation of the molecular structure and internal rotation of phenol and catechol. *J. Mol. Struct.: THEOCHEM* **1983**, *92*, 173−189.
(46) Parra, R. D.; Calderon, E. C. Planar vs non-planar structure of gaseous catechol in the S0 state: an ab initio study. *J. Mol. Struct.: THEOCHEM* **2004**, *682*, 235−240.
(47) Puebla, C.; Ha, T.-K. A theoretical study of conformations and rotational barriers in dihydroxybenzenes. *J. Mol. Struct.: THEOCHEM* **1990**, *204*, 337−351.
(48) Steiner, T. The Hydrogen Bond in the Solid State. *Angew. Chem., Int. Ed.* **2002**, *41*, 48−76.
(49) Bilton, C.; Allen, F. H.; Shields, G. P.; Howard, J. A. K. Intramolecular hydrogen bonds: common motifs, probabilities of formation and implications for supramolecular organization. *Acta Crystallogr. B* **2000**, *56*, 849−856.
(50) Infantes, L.; Motherwell, W. D. S. Hydrogen bond competition between chemical groups: new methodology and the Cambridge Structural Database. *Z. Kristallogr.* **2005**, *220*, 333−339.
(51) Jeffrey, G. A.; Saenger, W. *Hydrogen Bonding in Biological Structures*; Springer-Verlag: Berlin-Heibleberg, 1991; pp 425−451.
(52) Sarkhel, S.; Desiraju, G. R. N-H···O, O-H···O, and C-H···O hydrogen bonds in protein-ligand complexes: strong and weak interactions in molecular recognition. *Proteins* **2004**, *54*, 247−259.
(53) Steiner, T.; Schreurs, A. M. M.; Kanters, J. A.; Kroon, J. Water Molecules Hydrogen Bonding to Aromatic Acceptors of Amino Acids: the Structure of Tyr-Tyr-Phe Dihydrate and a Crystallographic Database Study on Peptides. *Acta Crystallogr. D* **1998**, *54*, 25−31.
(54) Steiner, T. Competition of hydrogen-bond acceptors for the strong carboxyl donor. *Acta Crystallogr. B* **2001**, *57*, 103−106.
(55) Jang, S. H.; Park, S. W.; Kang, J. H.; Lee, S. Computational Study of Catechol-$(H_2O)_n$ (n=1−3) Clusters. *Bull. Korean Chem. Soc.* **2002**, *32*, 1297−1303.
(56) Tripos. Benchware 3D Explore. Computer Program. 2006. 1699 South Hanley Rod. St. Louis, MO.
(57) Chertanova, L.; Pascard, C.; Sheremetev, A. X-ray investigation of glyoxime derivatives. V. Two isomers of 2-(thienyl)glyoxime. A database study of the geometry and hydrogen bonding of the oxime group. *Acta Crystallogr. B* **1994**, *50*, 708−716.
(58) Tchertanov, L.; Pascard, C. Statistical Analysis of Noncovalent Interactions of Anion Groups in Crystal Structures. II. Hydrogen Bonding of Thiocyanate Anions. *Acta Crystallogr. B* **1996**, *52*, 685−690.
(59) Tchertanov, L.; Pascard, C. Statistical Analysis of Noncovalent Interactions of Anion Groups in Crystal Structures. III. Metal Complexes of Thiocyanate and their Hydrogen-Donor Accepting Function. *Acta Crystallogr. B* **1997**, *53*, 904−915.
(60) Tchertanov, L. Understanding the Peculiarities of Azide and Thiocyanate Binding in Proteins: Use of the Small Molecule Structural Data. *J. Supramol. Chem.* **2000**, *12*, 67−91.
(61) Billich, A. S-1360 Shionogi-GlaxoSmithKline. *Curr. Opin. Investig. Drugs* **2003**, *4*, 206−209.
(62) Rowley, D. C.; Hansen, M. S.; Rhodes, D.; Sotriffer, C. A.; Ni, H.; McCammon, J. A.; Bushman, F. D.; Fenical, W. Thalassiolins A-C: new marine-derived inhibitors of HIV cDNA integrase. *Bioorg. Med. Chem.* **2002**, *10*, 3619−3625.
(63) Schiavoni, M. M.; Di Lorento, H. E.; Hermann, A.; Mack, H. G.; Ulic, S. E.; Della Védova, C. O. Keto-enol tautomerism in -ketoesters: CH3C(O)CHXC(O)OY (X = H, Cl; Y = CH3, C2H5). Vibrational analyses, NMR spectra and quantum chemical calculations. *J. Raman Spectr.* **2001**, *32*, 319−329.
(64) Bertolasi, V.; Gilli, P.; Ferretti, V.; G., G. Resonance-Assisted O-H···O Hydrogen Bonding: Its Role in the Crystalline Self-Recognition of beta-Diketone Enols and Its Structural and IR Characterization. *Chem.−Eur. J.* **1996**, *2*, 925−934.
(65) Madsen, G. K. H.; Iversen, B. B.; Larsen, F. K.; Kapon, M.; Reisner, G. M.; Herbstein, F. H. Topological Analysis of the Charge Density in Short Intramolecular O-H···O Hydrogen Bonds. Very Low Temperature X-ray and Neutron Diffraction Study of Benzoylacetone. *J. Am. Chem. Soc.* **1998**, *120*, 10040−10045.
(66) Schiøtt, B.; Iversen, B. B.; Madsen, G. K. H.; Larsen, F. K.; Bruice, T. C. Characterization of the Short Strong Hydrogen Bond in Benzoylacetone by ab Initio Calculations and Accurate Diffraction Experiments. Implications for the Electronic Nature of Low-Barrier Hydrogen Bonds in Enzymatic Reactions. *J. Am. Chem. Soc.* **1998**, *120*, 12117−12124.
(67) Gilli, P.; Ferretti, V.; Gilli, G. Hydrogen Bonding Models: Their Relevance to Molecular Modelling. In *Fundamental Principles of Molecular Modeling*; Kluwer Academic Publishers: Boston, 1996; p 249.
(68) Cleland, W. W.; Kreevoy, M. M. Low-barrier hydrogen bonds and enzymic catalysis. *Science* **1994**, 1887−1890.
(69) Frey, P. A.; Whitt, S. A.; Tobin, J. B. A low-barrier hydrogen bond in the catalytic triad of serine proteases. *Science* **1994**, *264*, 1927−1930.
(70) Karpfen, A. Cooperative Effects in Hydrogen Bonding. In *Advances in Chemical Physics*; Prigogine, S. A. R., Ed.; 2003; pp 469−510.
(71) Feng, M.; Patel, D.; Dervan, J. J.; Ceska, T.; Suck, D.; Haq, I.; Sayers, J. R. Roles of divalent metal ions in flap endonuclease-substrate interactions. *Nat. Struct. Mol. Biol.* **2004**, *11*, 450−456.
(72) Steitz, T. A. A mechanism for all polymerases. *Nature* **1998**, *391*, 231−232.
(73) Steitz, T. A. DNA polymerases: structural diversity and common mechanisms. *J. Biol. Chem.* **1999**, *274*, 17395−17398.
(74) Cowan, J. A. *The Biological Chemistry of Magnesium*; VCH: New York, 1995; p 254.
(75) Cotton, F. A.; Cotton, F. A.; Murillo, C. A.; Bochmann, M. *Advanced Inorganic Chemistry*; Wiley-Interscience: New York, 1999; p 1376.
(76) Danilewicz, J. C. Review of Reaction Mechanisms of Oxygen and Proposed Intermediate Reduction Products in Wine: Central Role of Iron and Copper. *Am. J. Enol. Vitic.* **2003**, *54*, 73−85.
(77) Pierpont, C. G. Studies on charge distribution and valence tautomerism in transition metal complexes of catecholate and semiquinonate ligands. *Coord. Chem. Rev.* **2001**, *216−217*, 99−125.
(78) Ribeiro da Silva, M. A. V.; Ferrão, C. C. H. Energetics of metal-oxygen bonds in metal complexes of β-diketones. *Pure Appl. Chem.* **1988**, *60*, 1225−1234.
(79) Pierpont, C. G.; Buchanan, R. M. Transition metal complexes of o-benzoquinone, o-semiquinone, and catecholate ligands. *Coord. Chem. Rev.* **1981**, *38*, 45−87.
(80) Kelly, M. D.; Mancera, R. L. A new method for estimating the importance of hydrogen-bonding groups in the binding site of a protein. *Comput.-Aided Mol. Des.* **2003**, *17*, 401−414.
(81) Ouali, M.; Laboulais, C.; Leh, H.; Gill, D.; Desmaele, D.; Mekouar, K.; Zouhiri, F.; d'Angelo, J.; Auclair, C.; Mouscadet, J. F.; Le Bret, M. Modeling of the inhibition of retroviral integrases by styrylquinoline derivatives. *J. Med. Chem.* **2000**, *43*, 1949−1957.
(82) Bruno, I. J.; Cole, J. C.; Edgington, P. R.; Kessler, M.; Macrae, C. F.; McCabe, P.; Pearson, J.; Taylor, R. New software for searching the Cambridge Structural Database and visualising crystal structures. *Acta Crystallogr. B* **2002**, *58*, 389−397.
(83) CCDC. Vista - A Program for the Analysis and Display of Data Retrieved from the CSD. 1994. 12 Union Road, Cambridge, England.
(84) Macrae, C. F.; Edgington, P. R.; McCabe, P.; Pidcock, E.; Shields, G. P.; Taylor, R.; Towler, M.; van de Streek, J. Mercury: visualization and analysis of crystal structures. *J. Appl. Crystallogr.* **2006**, *39*, 453−457.

JM061375J